Available online at www.sciencedirect.com
SCIENCE DIRECT®
Biochemical and Biophysical Research Communications 327 (2005) 49–56
BBRC
www.elsevier.com/locate/ybbrc

Quadruplex–duplex competition in the nuclease hypersensitive element of human *c-myc* promoter: C to T mutation in C-rich strand enhances duplex association

Kangkan Halder, Vidhi Mathur, Dipankar Chugh, Anjali Verma, Shantanu Chowdhury*

Institute of Genomics and Integrative Biology, CSIR, Mall Road, Delhi 110007, India

Received 22 November 2004
Available online 8 December 2004

Abstract

The nuclease hypersensitive element NHE III_1 is an important anti-cancer target as the transcription of oncogene *c-myc* is largely regulated by it. It has been postulated that regulatory control is mediated by G-quadruplex formation in the NHE anti-sense strand through a competition between the duplex and the quadruplex states. A mutation in the NHE has been implicated in cancer. In this study, the reported mutation has been characterized vis-à-vis the kinetics of *i*-tetraplex formation (in the sense strand) and its effect on duplex formation. We found that *i*-tetraplex formation was destabilized by ~1.4 kcal/mol ($\Delta\Delta G$ at 20 °C, pH 5.8). Observed hysteresis allowed us to analyze the kinetics of folding for the mutant (M3). Though we observed higher association ($\Delta E_{on} \approx -23.4$ kcal/mol) and dissociation ($\Delta E_{off} \approx 22.1$ kcal/mol) activation energies (at pH 5.3) for the wild-type (P1) tetraplex folding, the kinetics of folding and unfolding for M3 was somewhat faster at pH 5.3 and 5.8. Interestingly, Surface plasmon resonance (BIAcore) analysis of hybridization at pH 6.6 indicated a higher association constant for M3 ($\sim 22.5 \times 10^4\ M^{-1} s^{-1}$) than P1 ($\sim 3.2 \times 10^4\ M^{-1} s^{-1}$). The equilibrium dissociation constants also indicated favorable duplex association for M3 (~22.2 and ~190.6 nM for M3 and P1, respectively). We envisage that the increased affinity for the duplex state due to the mutation could play a functional role in the aberrant regulation of *c-myc*.

Keywords: *i*-Motif; NM23-H2; Hysteresis; Surface plasmon resonance; BIAcore; Hybridization kinetics

Human *c-myc* has been implicated in many malignant tumors [1,2]. *c-myc* expression is positively regulated by a promoter element designated nuclease hypersensitive element (NHE III_1) which corresponds to bases 2180–2212 in the human *c-myc* locus [3,4]. The NHE III_1 is guanine-rich in its anti-sense strand while the complementary sense strand is cytosine-rich. A secondary structure formed by the G-rich sequence in the NHE—the G-quadruplex has been implicated as a factor in regulation of *c-myc* [5,6]. Thus, postulated models of regulation entail a switching between the structural motif and duplex DNA [5,6]. In this context, the role of the complementary C-rich sense strand is less clearly understood; despite the observation that this strand adopts a stable tetraplex structure (*i*-motif) in solution [7]. C-tetraplexes are formed by the base pairing of hemiprotonated cytosine$^+$ and cytosine to form duplex structures, which are intercalated in an antiparallel orientation to form tetraplexes [8]. A pH-dependent equilibrium involving monomeric *i*-tetraplexes was first observed in a 17-mer C-rich fragment from human centromeric satellite III [9]. Intramolecular *i*-motifs were also observed in multiple dodecamer repeats implicated in progressive myoclonus epilepsy [10]. We recently found that the thermodynamic properties of *i*-tetraplex folding from *c-myc* NHE are

* Corresponding author. Fax: +91 11 2766 7471.
E-mail address: shantanuc@igib.res.in (S. Chowdhury).

0006-291X/$ - see front matter © 2004 Elsevier Inc. All rights reserved.
doi:10.1016/j.bbrc.2004.11.137

sensitive to change in pH and ionic strength [11]. This observation along with the finding that a G to A mutation in the anti-sense strand of the *c-myc* NHE has direct role in cancer [12] prompted us to explore the role of this mutation on *i*-tetraplex stability and tetraplex–duplex competition. In order to address this question we selected two mutant oligodeoxynucleotides. One (M3) harboring the C to T mutation (complementary to the reported G to A mutation) and a control (M2) with a C to T substitution in the previous cytosine tetrad stretch (see Materials and methods). M2 was chosen to see the effect of an identical mutation at an alternate position in the stem of the *i*-tetraplex (structure proposed in Fig. 8D of reference [7]). On studying the thermodynamic and kinetic folding properties of the oligodeoxynucleotide analogues we found that the mutants also formed the *i*-tetraplex structure in vitro. Surprisingly, both mutants showed increased kinetic association and dissociation with respect to the wild-type sequence making tetraplex folding thermodynamics unfavorable by ~1.2 kcal/mol ($\Delta\Delta G$ at 20 °C, pH 5.8). This is in contrast to the severe destabilization of the G-quadruplex due to the respective mutation on the G-rich strand [6]. Based on our results from kinetic analysis of hysteresis (UV denaturation/renaturation of folding) and hybridization using surface plasmon resonance (SPR), we believe that altered kinetics of C-tetraplex folding/unfolding effects duplex hybridization in the mutant, which may have implications on transcription factor binding and regulation of *c-myc*.

Materials and methods

The 31-mer oligodeoxynucleotides, wild-type P1: d(CCC CAC CTT CCC CAC CCT CCC CAC CCT CCC C) whose sequence corresponds to bases 2180–2210 of the human *c-myc* locus [4]; mutant M2: d(CCC CAC CTT CCT CAC CCT CCC CAC CCT CCC C); and mutant M3: (CCC CAC CTT CCC CAC CCT CCT CAC CCT CCC C), were obtained as HPLC purified from Sigma Genosys. Respective base substitutions in M2 and M3 are underlined. Single strand oligodeoxynucleotide concentration was determined using molar extinction coefficient ($\varepsilon_{260\ nm} = 7913$ (P1) and 7927 (M2 and M3) $M^{-1}cm^{-1}$) calculated according to Gray [13]. All experiments were performed in Robinson–Britton buffer (40 mM each of boric acid, acetic acid, and phosphoric acid, required pH was adjusted using NaOH).

CD measurements were performed on Jasco Spectropolarimeter (model J 715) equipped with a thermostat controlled cell holder of path length 1 cm. pH titrations were performed at 20 °C by addition of NaOH directly to 2 mL buffer (pH 4.8). A 30 min time interval was given after each NaOH addition for the reaction to reach equilibrium. pH was monitored using an Orion microelectrode. CD spectra were recorded from 220 to 400 nm with an averaging time of 3 s. Absorbance versus temperature denaturation/renaturation was performed on a Cary 400 (Varian) spectrophotometer equipped with Hitachi SPR-10 thermoprogrammer and temperature probe. Thermal denaturation was recorded at 260 nm and 295 nm with a heating rate of 0.25 °C/min. The equilibrium association constant K can be evaluated as $k_{on}/k_{off} = \alpha/(1-\alpha)$ for an intramolecular folding, where α is the fraction of oligodeoxynucleotides engaged as *i*-tetraplex.

Non-denaturing gel electrophoresis experiments were performed with the 31-mer oligodeoxynucleotides (P1, M2, and M3) 5′-end labeled with T4 polynucleotide kinase (New England Biolabs) and [γ-^{32}P]ATP. Experiments were performed in Robinson–Britton buffer (0.04 M each of boric acid, acetic acid, and phosphoric acid, required pH was adjusted using NaOH) as described before [11].

Analysis of hysteresis. Evaluation of thermodynamic parameters from denaturation curves requires that the process be in true equilibrium, which implies that denaturation and renaturation curves are coincident. However, this is not always the case. It has been observed that the thermal dissociation are largely shifted towards higher temperatures compared to association (on cooling). This behavior, a result of slow association and dissociation kinetics, has been previously described for *i*-tetraplex [14,15] and triple helix formation [16]. Hysteresis, in our case, was concentration independent, indicating a slow intramolecular process. Quantitative analysis was done as described before by Mergny and co-workers [15,16].

Hybridization kinetics using BIAcore. Surface plasmon resonance measurements were performed with BIAcore 2000 (BIAcore) system using streptavidin-coated sensor chips (Sensor chip SA, BIAcore). The 39-mer 5′-biotinylated sequence d(ATG CAT GCG GGG AGG GTG GGG AGG GTG GGG AAG GTG GGG) (Sigma Genosys) was immobilized on flow cell 2 to attain a binding of 1167 response units (RU) as described before [17]. Flow cell 1 was left blank as control to account for any signal generated due to bulk solvent effect or any other effect not specific to the DNA interaction, which was subtracted from the signal obtained in flow cell 2. All experiments were performed at 25 °C using running buffer (filtered and degassed 10 mM Hepes, 150 mM NaCl, 3 mM EDTA, and 0.005% surfactant IGEPAL) at pH 6.6 or 7.4. Oligo immobilized surface was exposed to the running buffer for at least 2 h at a flow rate of 5 μl/min for attaining folded/unfolded equilibrium on the chip surface. Analyte (P1 or M3) solutions at different concentrations (8–512 nM) in running buffer were injected (at 20 μl/min for 180 s) using automated protocol and dissociation from the surface was monitored for 300 s in running buffer. Surface regeneration after every cycle was done using 1 M NaCl in 50 mM NaOH, as the running buffer could not completely dissociate the complex from the surface. Mass transfer analysis done at varying flow rates (5, 20, and 50 μl/min) showed no significant difference in association rates. The association and dissociation constants were kinetically analyzed from the corresponding changes in response units using the integrated equations described previously [18]. Briefly, the dissociation phase of the interactions was analyzed using

$$R_t = [R_a \exp(-k_d t)] + R_\alpha, \tag{1}$$

where R_t is the observed response at time t, R_α is the expected response at infinite time, R_a is the amplitude of dissociation, and k_d is the dissociation rate constant. The association kinetics were analyzed using the equation

$$R_t = \{Ck_aR_{max}[1 - \exp(-(Ck_a + k_d)t)]/(Ck_a + k_d)\} + R_I, \tag{2}$$

where R_t is the observed response at time t, R_{max} is proportional to the concentration of active ligand on the surface, k_a is the association rate constant, k_d is the dissociation rate constant, R_I is a fitting parameter which is equivalent to response at initiation of injection ($t = 0$), and C is the concentration of analyte. We used the integrated non-linear least squares method for our analysis [18] instead of the more frequently used linear transformations [19,20] to directly analyze the primary data obtained from BIAcore and avoid parameter-associated errors due to linearization.

Equilibrium analysis was performed by plotting the response at equilibrium, obtained by subtracting the response of the control flow cell 1 from that of flow cell 2, against analyte concentration. The data were fit to the equation

$$RU_{eqb} = RU_{max}[\text{analyte}]/(K_D + [\text{analyte}]), \tag{3}$$

where RU_{eqb} is the measured response, RU_{max} is the maximum response, and K_D is the equilibrium dissociation constant for binding interaction.

Results and discussion

Effect of single nucleotide substitution on i-tetraplex formation

The stability of folded geometry under in vitro conditions was studied as a function of pH using CD spectroscopy of the oligodeoxynucleotides P1, M2, and M3. Fig. 1 shows CD scans at different pH for M3 where a characteristic positive (287 nm) peak and negative (254 nm) peak, with approximately half the amplitude, were observed. These features are consistent with a topology involving hemiprotonated cytosine–cytosine$^+$ base-paired tetrad motif as confirmed for P1 previously by us and others [7,11]. Similar spectral profiles were obtained for M2 and M3 also. Respective pH profiles were plotted by measuring change in ellipticity of the positive band at 287 nm (inset). It showed that the tetraplex fold was largely retained in the pH range 4.5–5.5 while further increase in pH resulted in unfolding to an unstructured single strand conformation. Observed transition mid points varied from pH 6.0 ± 0.2 (for P1), 5.8 ± 0.2 (M3) to 5.7 ± 0.2 (M2), indicating that the oligodeoxynucleotides with single nucleotide mutations needed lower pH for tetraplex stability, which could be due to differences in intercalation topology whereby smaller number of C–C$^+$ base pairs are involved in the stem in case of the mutants. It may be noted that the pH mid-titration value of 6.0 ± 0.2 for P1 is less than our previously reported value (~6.8 [11]), which could

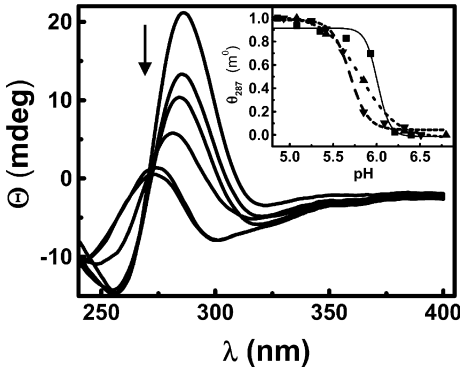

Fig. 1. CD spectra of the cytosine-rich oligonucleotide from *c-myc* promoter (P1) and mutants (M2 and M3) at various pH. Plot shows CD scans of M3 at pH 4.74, 5.09, 5.42, 5.85, 6.32, and 6.80, while arrow indicates trend with increasing pH. Inset depicts the ellipticity at 287 nm versus pH for P1 (squares), M2 (up triangles), and M3 (down triangles). All spectra were recorded with 2.0 μM oligonucleotide at 20 °C in 20 mM Robinson–Britton buffer; pH was adjusted using NaOH.

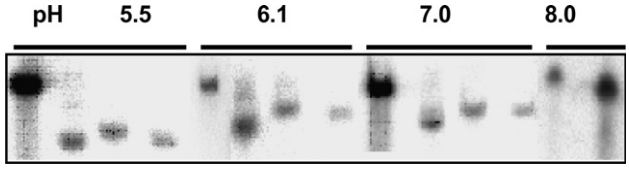

Fig. 2. Non-denaturing polyacrylamide gel electrophoresis of cytosine-rich 31-mer DNA from promoter site of human *c-myc*. Wild-type (P1, lanes 2, 6, 10, and 14), mutants (M2, lanes 3, 7, and 11) and (M3, lanes 4, 8, and 12), and control (dT31, lanes 1, 5, 9, and 13) were observed at different pH in Robinson–Britton buffer.

be due to the different buffer conditions used here, wherein NaOH was required for pH adjustment and is consistent with our previous finding that sodium ions destabilize the *i*-tetraplex [11]. The CD results were further confirmed by non-denaturing PAGE (Fig. 2). We observed that mobility of all the oligodeoxynucleotides was higher than the 31-mer dT or unfolded P1 (at pH 8, lane 14) between pH 5.5 and 7 indicating intramolecular folding. The existence of predominantly folded conformations at pH 7.0 was somewhat surprising based on the mid-transition points evaluated from CD and may be due to the different experimental protocols. The slight difference between unfolded P1 and dT31 at pH 8.0 may be due to the cytosine-rich sequence, a similar difference was observed with all the oligodeoxynucleotides under denaturing conditions (data not shown).

Thermodynamics of i-tetraplex folding

Thermodynamic stability of the oligodeoxynucleotides, which folded into the *i*-tetraplex, was characterized as a function of pH. The pHs (4.8, 5.3, and 5.8) were chosen such that P1, M2, and M3 would maintain a predominantly folded state at 20 °C. Transitions were observed to be cooperative and reversible, except for P1 and M3 at pH 5.3 and 5.8 where hysteresis was observed (Fig. 3). Table 1 summarizes the evaluated T_M. It was observed that largely stability of the folded motif decreased at higher pH as indicated by decreasing melting temperatures. This is consistent with earlier reports on stability of intercalated DNA [7,21] and supports the fact that stability may be primarily due to favorable interactions between hydrogen-bonded C$^+$·C base pairs as first indicated by Sponer et al. [22]. The observed trend on comparing P1, M2, and M3 indicated that at pH 5.3 the stability profiles varied considerably while it was within ±3 °C at the other pH. Thermodynamic parameters determined from profiles at 295 nm were identical (but inverse due to hypochromism on unfolding as cytosine protonation is lost [21]) within experimental error (data not shown). In all cases, T_M was concentration independent, indicating that folding of all the oligodeoxynucleotides was intramolecular.

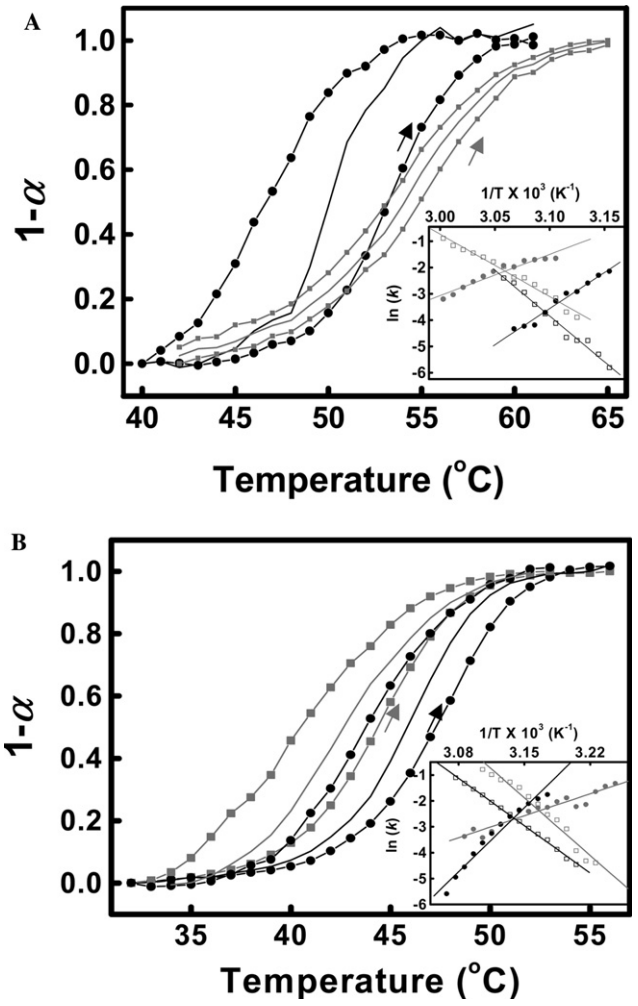

Fig. 3. Hysteresis and Arrhenius plot of the derived kinetic association (k_{on}) and dissociation (k_{off}) constants in 20 mM Robinson–Britton buffer with 3 μM P1 or M3. (A) Denaturation and renaturation curves for P1 (line with circles, in black) and M3 (line with squares, in grey) and inset shows the Arrhenius plot of k_{on} (filled circles) and k_{off} (open squares) for P1 (black) and M3 (grey) at pH 5.3. (B) Denaturation/renaturation curves and Arrhenius plot (inset) for P1 and M3 at pH 5.8. Symbols and colors as in (A). Simulated equilibrium profiles are shown as continuous lines with the respective hysteresis curves. (Using the k_{on} and k_{off} values determined at each temperature, equilibrium constant (k_{on}/k_{off}) at each temperature can be derived, and thus the fraction of oligodeoxynucleotide at equilibrium as a function of T, which were used to generate the simulated equilibrium curves. These curves would be attained if an 'infinitely' slow temperature gradient could be used.) Equilibrium T_M can be estimated from the crossing point between the E_{on} and E_{off} fits in the insets.

From the melting profiles, one could determine the mole fraction (α) of oligodeoxynucleotides engaged in tetraplex formation. The logarithm of equilibrium association constant K (expressed as $\alpha/(1-\alpha)$ for an intramolecular equilibrium) of the *i*-tetraplex can be plotted against $1/T$. Good linear fits were obtained with the experimental points ($r > 0.997$), indicating that the melting transition can be approximated to an all-or-none intramolecular equilibrium (data not shown). In the case of P1 and M3 where considerable hysteresis was observed the simulated equilibrium curve (discussed below) was used to obtain thermodynamic enthalpy and entropy parameters. Table 1 summarizes the representative thermodynamic parameters determined from the linear fits at 20 °C (where all oligodeoxynucleotides were in ordered form, as indicated by CD spectra) and pH 5.8. It was observed that M2 folding at pH 5.8 was enthalpically least favored ($\Delta H^0 = -86.72$ kcal/mol) and P1 was most favored ($\Delta H^0 = -97.01$ kcal/mol) while M3 had intermediate enthalpy of folding. In contrast, entropy was unfavorable for P1 with respect to M1 or M2 giving only a modest difference in the free energy of intramolecular association. Similarly, it was observed that folding at 20 °C was accompanied by favorable free energy terms resulting from characteristic compensation of favorable enthalpy and unfavorable entropy at all pH. Electrostatic stabilization as a result of $C \cdot C^+$ base pairing and favorable interactions between the protonated bases and the sugar-phosphates may result in favorable enthalpy of folding whereas unfavorable entropy could be due to loss of rotational degree of freedom by DNA monomers and counterions [23]. It is noteworthy that the single nucleotide mutations resulted in a significant increase in enthalpy of folding vis-à-vis the wild-type P1 oligodeoxynucleotides ($\Delta\Delta H^0 = 10.29$ and 7.42 kcal/mol for M2 and M3, respectively), which may be due to a change in the primary intercalation topology as a result of C to T mutations.

Analysis of non-reversible melting curves

For the oligodeoxynucleotides P1 and M3 melting profiles were not superimposable at pH 5.3 and 5.8. Hysteresis, in all cases, was confirmed by identical, superimposed profiles obtained in successive heating and cooling cycles. The cooling curves were shifted to lower temperature compared to heating curves. Thermodynamically irreversible folding/unfolding of *i*-tetraplex was reported previously in a number of cases [15,16]. We performed the experiments at different strand concentrations and at different heating and cooling rates (0.05 and 0.25 °C/min) to test whether hysteresis was due to an experimental artefact or not. Hysteresis was observed to be concentration independent consistent with an expected intramolecular process but dependent on the rate of heating and cooling. The separation between heating and cooling profiles was larger at increased heating/cooling rates.

Hysteresis profiles for P1 and M3 are shown in Fig. 3. A large hysteresis was observed for P1 at pH 5.3 (Fig. 3A) with respect to M3 and shapes of the denaturation/renaturation curves were also significantly different; P1 association/dissociation appeared to be largely 'less cooperative' than M3. k_{on} and k_{off} values as determined from hysteresis at pH 5.3 and 5.8 (Figs. 3A and

Table 1
Thermodynamic parameters (at 20 °C) upon folding at different pH obtained from thermal denaturation at 260 nm

	T_M			ΔH^{0b} (kcal/mol)	ΔS^{0b} (cal/mol/K)	ΔG^{0b} (kcal/mol)
	pH 4.8	pH 5.3[a]	pH 5.8[a]			
P1	65.5	50.0 (50.01 ± 2.50)	45.0 (45.65 ± 1.60)	−97.01 (−121.08)	−305	−7.67
M2	62.5	56.0	42.0	−86.72	−275	−6.08
M3	64.5	53.5 (53.86 ± 3.23)	43.0 (42.92 ± 2.58)	−89.59 (−86.95)	−284	−6.46

[a] Denaturation/renaturation for P1 and M3 were not superimposable at these pH. T_M and thermodynamic parameters were therefore extracted both from calculated equilibrium curve and kinetic analysis as shown in Fig. 2. Values in parentheses were obtained from Arrhenius plot.
[b] Thermodynamic parameters were determined at pH 5.8. T_M was determined from at least two replicates and is within 0.5 °C. ΔH^0 values are within 5%, ΔG^0 and ΔS^0 values are within 6%. Folding was observed to be concentration independent in the range 0.5–3 μM.

B, respectively) were plotted in the form of Arrhenius plots $\ln(k_{on})$ and $\ln(k_{off})$ versus $1/T$ (inset) as described previously [15,16]. Positive and negative slopes for k_{on} and k_{off}, respectively, were obtained in the temperature range where hysteresis was predominant. T_M (where $\alpha = 1/2$, $k_{on} = k_{off}$) is given by the intersection of the straight lines and are listed in Table 1. Derived values of k_{on} and k_{off} at each temperature were used to calculate the equilibrium association constant (k_{on}/k_{off}), which was used to determine α, the fraction of folded oligodeoxynucleotides at any temperature, and thus an equilibrium curve was simulated for samples showing hysteresis (shown as continuous line profiles in Fig. 3). The appearance of the simulated profile within the expected range between denaturation and renaturation profiles validated the intramolecular model used to derive Arrhenius parameters [16]. At pH 5.3, the activation energy E_{on} for both the oligomers was negative (-54.48 ± 2.93 and -31.10 ± 2.72 kcal/mol for P1 and M3, respectively), which is consistent with earlier reports and indicates a nucleation-zipping model of association [15,16]. A more negative E_{on} for P1 may indicate that additional base pairs are involved in the initial nucleation process in case of P1 as discussed in detail previously for *i*-tetraplex and triplex association [15,16]. Interestingly, it was observed that the k_{on} slope for M3 was shifted to predominantly higher values (inset), indicating that the association process was faster in the case of M3. The activation energy for dissociation E_{off} was positive in both cases (69.14 ± 3.0 and 46.99 ± 1.93 kcal/mol for P1 and M3, respectively), consistent with the nucleation-zipping model. The smaller E_{off} for M3 may be due to a lower number of total bases involved in the *i*-tetraplex formation [16]. The k_{off} profile of M3 was obtained at higher values indicating enhanced dissociation kinetics for M3.

In contrast to pH 5.3, at pH 5.8 M3 had a slightly lower melting temperature than P1 and the shapes of the profiles seem to be more alike (and also reflect more cooperativity in the heating/cooling process). The activation energy E_{on}, in this case, was -69.95 ± 4.05 and -24.01 ± 1.89 kcal/mol for P1 and M3, respectively. The reason for higher E_{on} in the case of P1, compared to pH 5.3, may be due to increased number of C–C^+ base pairs in the initial nucleation process at higher pH. This is expected considering the fact that pK_a of cytosine is ~5 [21] and relatively weaker cytosine hemiprotonation at pH 5.8 may require more C–C^+ base pairs to nucleate for tetraplex folding to occur.

The observed E_{off} parameters (51.86 ± 0.72 and 62.96 ± 3.60 kcal/mol for P1 and M3, respectively) indicated higher activation energy for M3 dissociation though the k_{off} slope shows increased kinetic dissociation with respect to P1 (inset). This enhanced kinetics may be due to an M3-intercalation topology involving smaller number of intercalated cytosines with respect to P1 [11]. The lower E_{off} for P1 with respect to pH 5.3 is consistent with weaker C–C^+ bonds at higher pH. But the relatively higher E_{off} observed for M3 at pH 5.8 is interesting and may point towards stabilizing factors other than cytosine hemiprotonation like inter- or intraloop interactions which could be favored at higher pH [9]. The difference in standard molar enthalpy of formation ($\Delta\Delta H^0 \simeq -34.85$ kcal/mol) favors P1 folding as in pH 5.3. Taken together, the kinetics of folding/unfolding of M3 is pH dependent and distinct with respect to P1. M3 has both faster association and dissociation rates of folding.

Surface plasmon resonance analysis of hybridization

Our finding that the intramolecular tetraplex folding due to the mutation was significantly different prompted us to investigate the potential for hybridization of M3 to the complementary G-rich strand vis-à-vis P1. We used SPR for this study as this technique has been observed to be highly effective in characterization of interaction events in terms of kinetic parameters of association and dissociation rate constants [18–20]. Our experiments were performed at pH 6.6. This pH was chosen so that the effect of kinetic folding of tetraplex species on hybridization could be observed without disrupting the formation of duplex DNA to a large extent. Under our experimental conditions we observed that only about one-fourth of the surface bound G-rich strands (~250 RU) could be hybridized under saturating

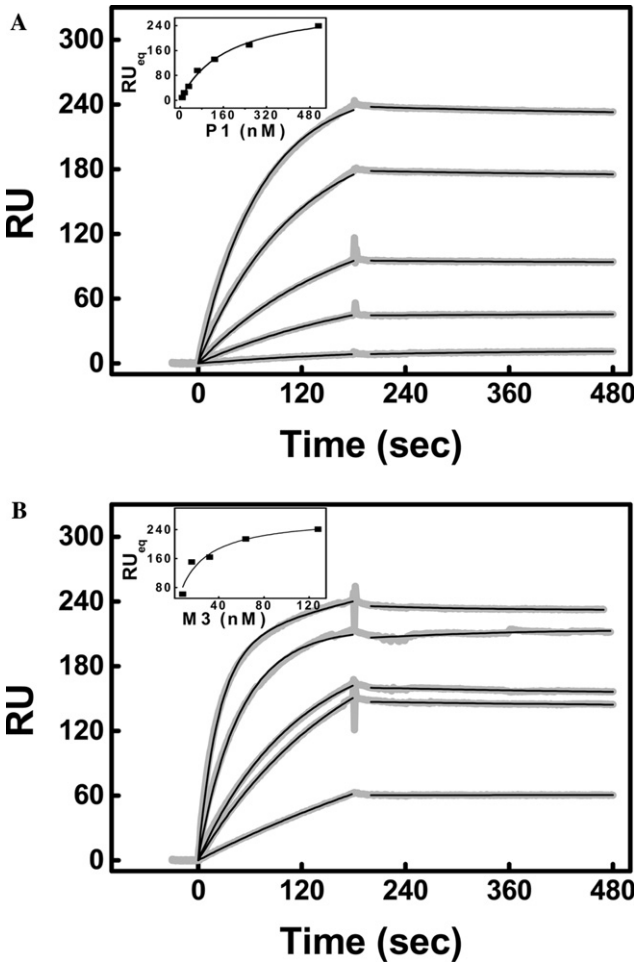

Fig. 4. Surface plasmon resonance sensorgrams and equilibrium binding isotherms of P1 and M3 hybridization to G-rich anti-sense strand in the *c-myc* promoter region. (A) Sensorgram of P1 (8, 32, 64, 256, and 512 nM) in flow buffer with binding isotherm (inset); (B) sensorgram of M3 (8, 16, 32, 64, and 128 nM) in running buffer with binding isotherm (inset). Binding isotherms were constructed using *RU* values from steady-state region of SPR sensorgrams versus analyte concentration. Grey lines were experimentally obtained and black lines were fitted using Eqs. (1) and (2); binding isotherms were fitted to Eq. (3). M3 at 128 nM showed best fits with biphasic association and dissociation as described before [19]; the observed constants were ($k_{a1} = 28{,}756$ and $k_{a2} = 20{,}020\ M^{-1}s^{-1}$ ($\pm 20\%$), $k_{d1} = 0.00693$ and $k_{d2} = 0.003\ s^{-1}$). All experiments were at 25 °C in 10 mM Hepes, pH 6.60, 150 mM NaCl, 3 mM EDTA, and 0.005% IGEPAL.

Table 2
Surface plasmon resonance analysis of P1 and M3 hybridization with the G-rich sequence from *c-myc* promoter at pH 6.6

	Kinetic analysis[a]			Equilibrium analysis
	k_d ($\times 10^{-3}\ s^{-1}$)	k_a ($\times 10^4\ M^{-1}s^{-1}$)	K_D ($\times 10^{-9}$ M)	K_D ($\times 10^{-9}$ M)
P1	3.5	3.2	110.6	190.6
M3	6.1	22.5	27.1	22.2

[a] Typical error levels for the k_d values are within $\pm 16\%$, k_a values within $\pm 23\%$ and K_D (equilibrium dissociation) within $\pm 10\%$.

concentrations of P1 or M3. This may be due to the presence of folded G-quadruplex structures, formed by this sequence [5], on the BIAcore chip surface, which could be inactive towards hybridization under our experimental conditions. Figs. 4A and B show the SPR sensorgrams with increasing concentrations of P1 and M3 (analyte, in solution), respectively, when passed over a fixed amount of the surface-immobilized complementary G-rich sequence. Inset shows the maximal equilibrium response plotted against the concentration of respective analyte, which gives the equilibrium dissociation constant K_D for hybridization. Interestingly, it was observed from equilibrium analysis that M3 binds with almost ninefold higher affinity than P1 (Table 2). Considering the fact that M3 harbors a mismatch (C to T mutation) with respect to the immobilized strand it was expected that P1 would have higher affinity, contrary to the observed result. Similarly, kinetic analysis of association and dissociation from the sensorgrams indicated a sevenfold lower association and about twofold lower dissociation in the case of P1. Best fits were obtained on considering monophasic association and dissociation (Fig. 4, with residuals within ± 2 response units in both cases), indicating that the interaction was primarily a two-state phenomenon. It may be noted that hybridization to the G-rich complementary strand, in case of folded motifs, necessitates opening of the intramolecular folding and/or interaction of a critical number of exposed bases in the folded motif to initiate duplex formation. Thus, the observed results may be explained considering interaction of intramolecularly folded P1 and M3 where the kinetics of unfolding for M3 being faster than P1, as deduced from hysteresis profiles, gives higher observed rate of hybridization. This is consistent with non-denaturing PAGE analysis of P1 and M3, which shows folded conformation to be predominant at between pH 6 and 7 (Fig. 2). However, the observed mid-transition points in CD indicate the presence of unfolded structures, which would, in principle, require at least a three-state model of interaction and a biphasic interaction profile. This was not observed except at high concentration (128 nM) of M3, which we believe, could be due to the formation of higher order structures. The reasons for discrepancy in CD and PAGE results are not very clear to us; the difference in experimental protocol followed for these experiments may be responsible. The above conclusion is further supported by the fact that the equilibrium dissociation constants at pH 7.4 are 9.62 ± 1.33 nM and 23.29 ± 1.67 nM for P1 and M3, respectively (data not shown). Here both P1 and M3 are expected to be predominantly unfolded and, as expected, higher affinity was observed for P1. The lower value for M3 could be due to one mismatch in M3. This difference is in accordance with a previous report of SPR analysis of mismatched hybridization [20]. The observed dissociation

constants at pH 6.6 showed about twofold higher dissociation for M3, as expected because of the single base mismatch in M3. Both the observed association and dissociation constants for hybridization with unfolded strands were roughly 10-fold higher than previously reported values for DNA–DNA hybridization [20]. The higher association constants may be due to the significantly higher GC% in the sequence that we have studied but this may be offset at the dissociation stage by the propensity of the G-rich strand to fold into a stable intramolecular motif thereby resulting in higher dissociation of the duplex. Duplex formation between P1 or M3 and the G-rich strand was independently observed using both CD and non-denaturing PAGE (data not shown).

Our study is significant as relatively few reports have been published [24–27] on nucleic acid interactions using the SPR technique and none has observed the effect of folded tetraplex structures vis-à-vis mismatched bases on hybridization. As we see, clearly this method is sensitive and reproducible enough to not only discriminate between mismatch hybridization (as observed by us here and others [20]) but could also be used to observe the effect on hybridization of single stranded folded motifs. Taken together, our SPR analysis indicates that the higher thermodynamic stability of folded P1 plays a major role in determining duplex formation at pH 6.6 whereby a slower association is observed relative to M3 though M3 harbors the point mismatch. M3 wins in duplex association by virtue of its relatively less thermodynamic stability and faster folding/unfolding kinetics. However, no significant difference in binding, other than due to mismatch hybridization, was observed at pH 7.4.

The thermodynamic parameters evaluated from Arrhenius plot for M3 and P1 give important clues to the intercalation topology though detailed structural elucidation by NMR or X-ray crystallography is required to confirm these aspects. In view of the previously proposed intercalation topology for P1 (with eight $C–C^+$ bonds) the observed enthalpy decrease of 121.08 kcal/mol (Table 1) indicates a favorable enthalpic contribution of $\sim$15 kcal/mol per $C–C^+$ bond formed, which is higher than the reported value of about -9 to -12 kcal/mol [21] and may be because of additional intraloop A·T bonding pairs possible in this structure [11]. It is noteworthy that both M2 and M3 show significantly lower enthalpic decrease due to folding (Table 1), which could be due to a change in the intercalation topology whereby only six $C–C^+$ pairs may be involved. This topology would be consistent with the observed higher kinetic folding/unfolding (except during folding at pH 5.8, where it is somewhat similar) in case of M3 as the nucleation-zipping model would favor faster kinetic association and dissociation with a tetrad core involving lesser number of hemiprotonated cytosines. SPR interaction studies support above conclusions. Our findings augment previous reports suggesting formation of different topologies consisting of six or eight $C–C^+$ pairs in the core of the *i*-tetraplex formed by the *c-myc* NHE [7]. We believe that in the mutants intercalation topology may be forced to change as one C to T mutation decreases the number of available cytosines for intercalation.

Biological implications

It is known that the *i*-motif structure is formed by natural sequences and recent observations indicate few proteins that could selectively interact with repeats of the telomeric cytosine-rich strand, possibly in the *i*-motif form [28]. This includes a 40 kDa nuclear protein of HeLa cells [29]; ST-1 from *Trypanosome brucei* [30]; qTBP42 in rat hepatocytes [31] while two nuclear proteins, hnRNP K and ASF/SF2, bind to telomeric cytosine-rich strand [32]. In vitro evidence of cytosine-rich repeats from vertebrate telomere [33] and human centromere [9] forming *i*-motif has been observed and the implications in biology discussed in terms of a regulatory role. In this context, a functional role of the cytosine-rich promoter region of *c-myc* cannot be ruled out where structural motifs stabilized by intracellular conditions may be regulatory in nature. Thus, the effect of single nucleotide substitutions affecting structure could be significant. The fact that the complementary G-rich strand once separated from the duplex state adopts tetraplex structures which undergo dramatic destabilization on single base substitution [34], with possible physiological consequences [6,12], is consistent with this idea.

In the context of our results, the implications of the (C to T) mutation on the dynamics of *i*-tetraplex stability and its consequence on duplex formation could be significant. Considering the evidence of strand separation and subsequent G-tetraplex formation playing a significant role in *c-myc* expression [5,6], any competing event which increases or decreases affinity for hybridization could have wider implications. The enhanced affinity for the duplex state by the mutant as observed in this study, along with the already destabilized G-quadruplex structure (due to the mutation), would give a predominantly duplex state of the NHE. This will disturb the postulated tetraplex–duplex switching model [6] as a control mechanism for regulation resulting in anomalous *c-myc* expression.

Acknowledgments

S.C. acknowledges Prof. Samir K. Brahmachari for constant support and CSIR for funding this research. K.H., V.M., and A.V. acknowledge research fellowship

from CSIR. We thank Souvik Maiti and other members of our group for many helpful discussions.

References

[1] C.A. Spencer, M. Groudine, Adv. Cancer Res. 56 (1991) 1–48.
[2] L.M. Facchini, L.Z. Penn, FASEB J. 12 (1998) 633–651.
[3] U. Siebenlist, L. Hennighausen, J. Battey, P. Leder, Cell 37 (1984) 381–391.
[4] C. Gazin, D.D. Dupont, A. Hampe, J.M. Masson, P. Martin, D. Stehelin, F. Galibert, EMBO J. 3 (1984) 383–387.
[5] T. Simonsson, P. Pecinka, M. Kubista, Nucleic Acids Res. 26 (1998) 1167–1172.
[6] A. Siddiqui-Jain, C.L. Grand, D.J. Bearss, L.H. Hurley, Proc. Natl. Acad. Sci. USA 99 (2002) 11593–11598.
[7] T. Simonsson, M. Pribylova, M. Vorlickova, Biochem. Biophys. Res. Commun. 278 (2000) 158–166.
[8] K. Gehring, J.L. Leroy, M. Gueron, Nature 363 (1993) 561–565.
[9] S. Nonin-Lecomte, J.L. Leroy, J. Mol. Biol. 309 (2001) 491–506.
[10] S.S. Pataskar, D. Dash, S.K. Brahmachari, J. Biomol. Struct. Dyn. 19 (2001) 307–313.
[11] V. Mathur, A. Verma, S. Maiti, S. Chowdhury, Biochem. Biophys. Res. Commun. 320 (2004) 1220–1227.
[12] C.L. Grand, T.J. Powell, R.B. Nagle, D.J. Bearss, D. Tye, M. Gleason-Guzman, L.H. Hurley, Proc. Natl. Acad. Sci. USA 101 (2004) 6140–6145.
[13] D.M. Gray, S.H. Hung, K.H. Johnson, Methods Enzymol. 246 (1995) 19–34.
[14] J.L. Leroy, M. Gueron, J.L. Mergny, C. Helene, Nucleic Acids Res. 22 (1994) 1600–1606.
[15] J.L. Mergny, L. Lacroix, Nucleic Acids Res. 26 (1998) 4797–4803.
[16] M. Rougee, B. Faucon, J.L. Mergny, F. Barcelo, C. Giovannangeli, T. Garestier, C. Helene, Biochemistry 31 (1992) 9269–9278.
[17] S. Maiti, N.K. Chaudhury, S. Chowdhury, Biochem. Biophys. Res. Commun. 310 (2003) 505–512.
[18] D.J. O'Shannessy, M. Brigham-Burke, K.K. Soneson, P. Hensley, I. Brooks, Anal. Biochem. 212 (1993) 457–468.
[19] R. Karlsson, A. Michaelsson, L. Mattsson, J. Immunol. Methods 145 (1991) 229–240.
[20] K.K. Jensen, H. Orum, P.E. Nielsen, B. Norden, Biochemistry 36 (1997) 5072–5077.
[21] J.L. Mergny, L. Lacroix, H. Xiaogang, J.L. Leroy, C. Helene, J. Am. Chem. Soc. 117 (1995) 8887–8898.
[22] J. Sponer, J. Leszczynski, V. Vetterl, P. Hobza, J. Biomol. Struct. Dyn. 13 (1996) 695–706.
[23] J. Gallego, E.B. Golden, D.E. Stanley, B.R. Reid, J. Mol. Biol. 285 (1999) 1039–1052.
[24] P. Nilsson, B. Persson, M. Uhlen, P.A. Nygren, Anal. Biochem. 224 (1995) 400–408.
[25] L.S. Wright, M.M. Harding, Anal. Biochem. 282 (2000) 70–79.
[26] R. Corradini, G. Feriotto, S. Sforza, R. Marchelli, R. Gambari, J. Mol. Recognit. 17 (2004) 76–84.
[27] S. Sawata, E. Kai, K. Ikebukuro, T. Iida, T. Honda, I. Karube, Biosens. Bioelectron. 14 (1999) 397–404.
[28] M. Gueron, J.L. Leroy, Curr. Opin. Struct. Biol. 10 (2000) 326–331.
[29] E. Marsich, L.E. Xodo, G. Manzini, Eur. J. Biochem. 258 (1998) 93–99.
[30] J.E. Eid, B. Sollner-Webb, Mol. Cell. Biol. 15 (1995) 389–397.
[31] G. Sarig, P. Weisman-Shomer, R. Erlitzki, M. Fry, J. Biol. Chem. 272 (1997) 4474–4482.
[32] L. Lacroix, H. Lienard, E. Labourier, M. Djavaheri-Mergny, J. Lacoste, H. Leffers, J. Tazi, C. Helene, J.L. Mergny, Nucleic Acids Res. 28 (2000) 1564–1575.
[33] A.T. Phan, M. Gueron, J.L. Leroy, J. Mol. Biol. 299 (2000) 123–144.
[34] L. Zhu, S.H. Chou, B.R. Reid, Proc. Natl. Acad. Sci. USA 93 (1996) 12159–12164.